Monodisperse Five-Nanometer-Sized Detonation Nanodiamonds Enriched in Nitrogen-Vacancy Centers

Mono-disperse five-nanometer-sized detonation nanodiamonds enriched in Nitrogen-Vacancy (NV^-) centers

https://doi.org/10.1021/acsnano.8b09383

Published in: ACS Nano, 13(6), 6461 - 6468 (2019).

Daiki Terada[1,2], Takuya F. Segawa*[1,3], Alexander I. Shames[4], Shinobu Onoda[5], Takeshi Ohshima[5], Eiji Ōsawa[6], Ryuji Igarashi[1,2], Masahiro Shirakawa[1,2]

1 Department of Molecular Engineering, Graduate School of Engineering, Kyoto University, Nishikyo-Ku, Kyoto 615-8510, Japan.

2 Institute for Quantum Life Science, National Institutes for Quantum and Radiological Science and Technology, 4-9-1, Anagawa, Inage-Ku, Chiba 263-8555 Japan.

3 Laboratory for Solid State Physics, Eidgenössische Technische Hochschule (ETH) Zürich, CH-8093 Zürich, Switzerland.

4 Department of Physics, Ben-Gurion University of the Negev, 8410501 Beer-Sheva, Israel.

5 National Institutes for Quantum and Radiological Science and Technology, 1233 Watanuki, Takasaki, Gunma 370-1292, Japan.

6 NanoCarbon Research Institute, AREC, Shinshu University, Ueda, Nagano 386-8567, Japan.

* E-mail: segawat@ethz.ch

ABSTRACT

Nanodiamonds containing negatively-charged nitrogen-vacancy (NV^-) centers are versatile nano-sensors thanks to their unique optical and spin properties. While currently most fluorescent nanodiamonds in use have at least a size of a few tens of nanometers, the challenge lies in engineering the smallest size nanodiamonds containing a single NV^- defect. Such a tiny nanocrystal with a single NV^- center is an "optical spin label" for biomolecules, which can be detected in a fluorescence microscope. In this paper, we address two key issues towards this goal using detonation nanodiamonds (DND) of 4-5 nm in size. The DND samples are treated first with electron irradiation to create more vacancies. With the aid of electron paramagnetic resonance (EPR) spectroscopy, we confirm a steady increase of negatively-charged NV^- centers with higher fluence. This leads to a four times higher concentration in NV^- defects after irradiation with 2 MeV-electrons at a fluence of 5×10^{18} e^-/cm^2. Interestingly, we observe that annealing of DND does not increase the number of NV^- centers, which is in contrast to bulk diamond and larger nanodiamonds. Since DND are strongly aggregated after the irradiation process, we apply a boiling acid treatment as a second step to fabricate mono-disperse DND enriched in NV^- centers. These are two important steps towards "optical spin labels" having single digit nanometer range size that could be used for bioimaging and nanosensing.

Keywords:

nanodiamonds, detonation nanodiamonds (DND), nitrogen-vacancy center (NV^- center), electron irradiation, annealing, electron paramagnetic resonance (EPR), optically-detected magnetic resonance (ODMR)

The negatively-charged nitrogen-vacancy (NV^-) center in diamond is the only system available today, where single electron spins can be detected at room temperature[1] and their coherence can be manipulated[2] over a lifetime of up to milliseconds.[3] This enormous gain in sensitivity, delivered by the combination of optical spin pumping and detection, is standing out from conventional nuclear magnetic resonance (NMR), magnetic resonance imaging (MRI) or electron paramagnetic resonance (EPR) techniques.[4] Numerous physical properties of the environment are encoded in the optical and magnetic resonance spectra of NV^- centers, enabling the detection of temperature,[5,6] magnetic[7,8] and electric fields,[9] to mention only a few.[10] Such a versatile sensor can be reduced to the nanoscale when NV^- centers are incorporated into nanometer-sized diamond crystals.[11] Low cytotoxicity and the remarkable photostability of the fluorescence from NV^- centers in 100 nm-sized crystals provided two major advantages compared to other fluorophores[11] and made nanodiamonds the ideal candidates for being unique nanoscale sensors inside living cells. Recently, sophisticated optically-detected magnetic resonance (ODMR) experiments presented novel methods to track the three-dimensional orientation of the nanodiamonds[12] or measure their surrounding temperature[13,14] in living cells.

While many unprecedented biophysical experiments can be expected in the near future based on nanodiamonds having sizes down to a few tens of nanometers, other targets will remain beyond reach if the nanodiamond size cannot be further reduced. If a NV^--containing nanodiamond should be used as a label for a single biomolecule such as a protein or a nucleic acid, its size should be at least comparable to the size of the biomolecule of interest. Accordingly, a size in the order of the famous green fluorescent protein (GFP)[15] would be highly desirable. A single-digit nanodiamond (having a size below 10 nm) would fulfill this criterion. This would open up the way to look at the molecular rotation of the ATP synthase[12] or study many other biophysical processes on a single-

molecule level in a natural environment that are unobservable today. Inspired from the huge success of EPR spectroscopy combined with site-directed spin labeling,[16] it would be a dream to replace those electron spin labels with tiny nanodiamonds carrying a single NV^- center to realize the step from large ensemble to single-molecule experiments. Furthermore, some cellular compartments like the cell nucleus are only accessible for very small particles. Some fluorescence or ODMR experiments like super-resolution imaging[17,18] are based on the measurements of a single NV^- defect and cannot be implemented on an NV^- ensemble in a larger nanodiamond. Finally, small nanodiamonds are essential for nanoscale sensing since the sensitivity is limited by the distance between NV^- centers and external spins.

Such small nanodiamonds can be either manufactured by the detonation method followed by destruction of their extremely tight agglutinates by attrition milling[19] or by using a laser-heated diamond anvil cell.[20] The latter method produces only minute amounts so far and the former is the only method suited for large-scale production at the moment. In this work, we are using detonation nanodiamonds (DND) with a uniform diameter of 4-5 nm.[19] NV^- centers in DND were first directly observed ten years ago by Plakhotnik and co-workers by time-resolved photoluminescence spectroscopy.[21] They suggested that sp^2 carbon on the surface can quench the luminescence from NV^- defects, showed an improved performance after surface oxidation and estimated that only about 1 per (15,000 ± 7,000) DND would contain an NV^- center corresponding to about 0.005-0.012 ppm.[22] While it is well known that the nitrogen concentration in DND is as high as 2-3 at% over the whole particle,[23] it is still under debate, if such high nitrogen concentrations can be found as well in the inner diamond core.[24–26] The smallest nanoparticles made from type Ib diamond that showed ODMR signal from NV^- centers had a mean particle size of about 8 nm.[27] Similar experiments in DND showed a striking difference between “covered” nanodiamonds inside

aggregates or a polymer film (poly-vinyl alcohol) and "naked" nanodiamonds surrounded by air: while the former showed stable fluorescence enabling to record ODMR spectra, the latter showed fluorescence blinking where no ODMR signal could be observed.[28] This might be related to the charge state conversion between negatively-charged NV^- and neutral NV^0 defects, where in the proximity of the particle surface, the equilibrium is shifted more towards the neutral species.[29] However, only the negatively-charged NV^- defect with an electron spin triplet ground state ($S = 1$) is ODMR active.[10]

Considering all these points, we see three key challenges that must be overcome before DND become a new generation of "optical spin labels": (1) the low concentration of NV^- centers in DND, (2) the strong aggregation of NV^--containing DND and (3) surface-induced charge instability of NV^- centers in isolated DND. In this work, we present solutions to overcome these challenges. By electron irradiation,[30] the number of NV^- defects increased through the creation of more lattice vacancies. With the aid of EPR spectroscopy,[31] we quantify the increase of NV^- centers' content in DND under three different irradiation fluences. At the highest fluence applied in this study (5×10^{18} e^-/cm^2) we estimate a 3.9-fold increase in NV^- centers with respect to non-irradiated DND. We report for the first time that annealing at 800 ºC for 2 h under vacuum has no influence on the number of NV^- defects in DND. Annealing has the purpose of rendering the vacancies mobile so as to create new NV centers. After electron irradiation (and also annealing), DND form tight aggregates that cannot be dispersed by high-power sonication alone. Graphitization of diamond carbon,[32] bridging of chemical bonds[33] and annealing effects due to beam heating[34] are known reactions induced by electron irradiation. By treating the DND with boiling acid (H_2SO_4:HNO_3 = 3:1, 125 °C)[35] the particles are redispersed. While the frequently used oxidation in air can remove sp^2 carbon on the DND surface, this step again leads to tightly aggregated DND caused by the

complete removal of water at high temperature.[36] We confirm that only the last oxidation step by acid makes ODMR signals in nanodiamond aggregates reappearing. All these three steps lead to mono-disperse DND enriched in NV^- centers.

RESULTS AND DISCUSSION

In order to increase the number of NV^- centers in DND, DND were irradiated with 2 MeV-electrons at different fluences (1×10^{18} e^-/cm^2, 3×10^{18} e^-/cm^2, 5×10^{18} e^-/cm^2). To estimate the relative concentration between NV^- centers in different DND samples, we characterized the samples using continuous-wave (CW) EPR spectroscopy. While the signal around g = 2 is dominated by an intense relatively narrow (line width ΔH_{pp} ~1 mT) singlet signal, largely stemming from dangling bonds (S = 1/2), an additional signal was recently attributed to the so-called "forbidden" $\Delta M_S = 2$ transition between Zeeman levels of the triplet (S = 1) NV^- centers that can be found at about g = 4.24(1) when measuring at the microwave X-band frequency in use (9.87 GHz).[37,38] In this "half-field" region (g ~ 4, relating to the half of the magnetic field value corresponding to signals of primary paramagnetic species like dangling bonds observed at g = 2.00), a second signal around g = 4.00(1) appears, which was assigned to another "forbidden" transition stemming from an S = 1 electron spin species in coupled dangling bonds.[31] Such an effect, where the EPR line corresponding to the "forbidden" transition in a powder spectrum is less broadened than conventional $\Delta M_S = 1$ "allowed" lines due to the strong orientation dependence of the spin-Hamiltonian parameters, is well known for EPR species in the triplet state.[39] Importantly, it was demonstrated that an estimation on the number of NV^- centers in nanodiamond powders is possible by double integration of the "forbidden" line.[31] Since such "forbidden" lines in the EPR

spectra of polycrystalline samples exist only for a spin $S \geq 1$ species, this method selectively measures the ODMR-active negatively-charged NV^- but not the neutral NV^0 centers having $S = 1/2$ (which have never been observed by EPR in its ground state).[40] The content of NV^- centers in DND was increased 1.8-fold by electron irradiation with a fluence of 1×10^{18} e^-/cm^2, 2.4-fold with 3×10^{18} e^-/cm^2 and 3.9-fold with 5×10^{18} e^-/cm^2 with respect to the non-irradiated DND sample (Fig. 1(a), (b) and Fig. S1 for all EPR spectra). All increment factors have an experimental error of ± 15%, showing a significant increase in the concentration of NV^- centers. Looking at these four data points, a saturation in the curve of the NV^- concentration is not yet seen and therefore, a further increase by larger fluences can be expected (Fig 1 (a)). Surprisingly, the amount of NV^- centers in DND was not affected by annealing at 800 °C for 2 h under vacuum (Fig. 1 (a), (c) and Fig. S1). This negative result was confirmed for both, non-irradiated and irradiated DND. High-energy electron or ion irradiation followed by annealing is a standard process to increase the number of NV^- centers in bulk diamond and nanodiamonds.[41] Since such an effect was only observed in DND so far, a size-dependent origin seems most obvious. We make two complementary attempts to explain this "anomalous" behavior. On one hand, annealing per se could be ineffective for DND due to their small size. In this case, most of the vacancies would arrive at the crystal surface before having the chance to pair with a single nitrogen defect.[21] On the other hand, annealing through high temperatures could have already fully taken place during electron irradiation or the DND synthesis, respectively. In that case, all possible NV^- centers would have already formed before the subsequent annealing process. This hypothesis relies on a strong irradiation-induced temperature rise for very small-sized nanoparticles[42], whereby its validity remains unclear since the particles are aggregated during this process.

The samples were further characterized by transmission electron microscopy (TEM) and diffuse reflectance infrared Fourier transform spectroscopy (DRIFTS) to monitor chemical changes induced by the electron beam. TEM images with a resolution of 0.1 nm show ca. 5 nm-sized diamond nanocrystals for all samples with no remarkable difference (Fig. 2(a)). Since a detection of sp^2 layers was not possible, we assume, if at all, only single layers for graphene or sp^2 carbon are covering the nanodiamond surface. Most importantly, the diamond structure was retained during electron irradiation as confirmed by selected-area electron diffraction (SAED) shown in Fig. 2 (a). In contrast, significant changes induced by the electron irradiation process on the nanodiamond surface were observed in the DRIFT spectra. While the C-H vibrations (2800-3000 cm^{-1}) disappear during the electron irradiation, C=O and C-O or C-O-C vibrations (1770 and 1000-1350 cm^{-1}, respectively[43]) are enhanced in the DRIFT spectra (Fig. 2 (b)). The formation of C=O and C-O-C groups was previously observed on irradiated carbon nanotubes leading to covalent bridges between adjacent tubes.[33] In our case, C-O-C groups may be formed between adjacent DND or on the DND surface. At the same time, the zeta potential was inverted from +41 ± 5 mV for the non-irradiated sample to -46 ± 15 mV for the 5×10^{18} e^-/cm^2 irradiated sample after the boiling acid treatment.

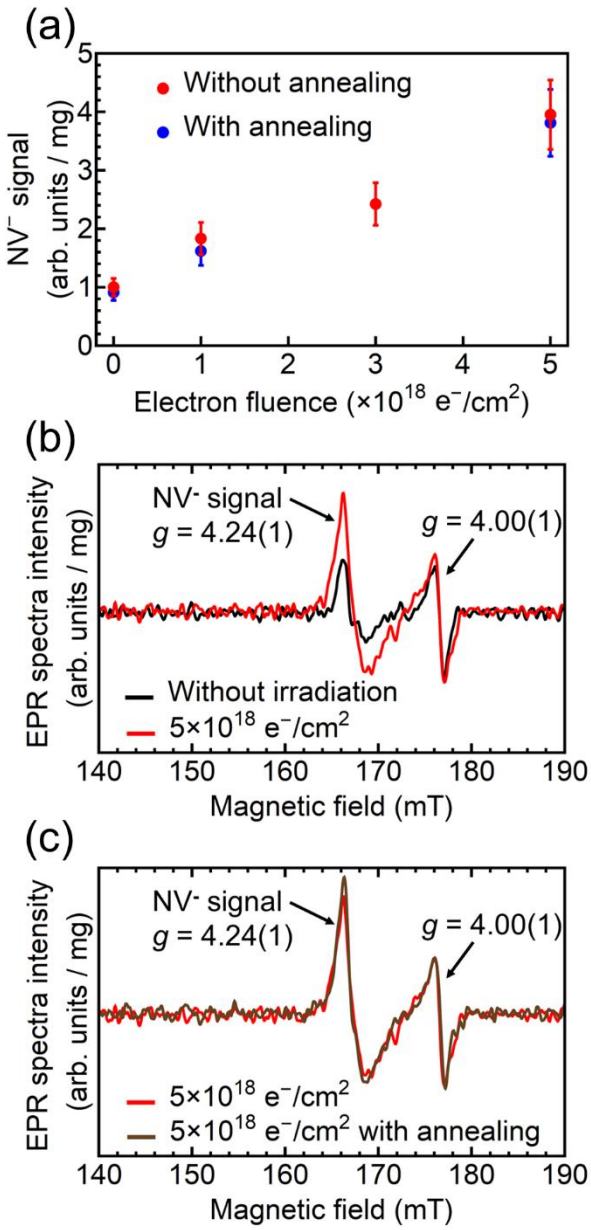

Figure 1. Effect of electron irradiation on NV^- centers in DND. (a) Relative quantification of NV^- defects by EPR for non-irradiated and electron irradiated DND normalized per weight. Red dots are before, blue dots are after annealing, respectively. All measurements have an error of ± 15 %. The NV^- signal for the non-irradiated DND before annealing was normalized to 1. (b) Half-field EPR spectra after baseline correction comparing non-irradiated (black) and 5×10^{18} e^-/cm^2 irradiated (red) DND (both after boiling acid treatment) showing a significant difference in

intensity. (c) Half-field EPR spectra after baseline correction comparing 5×10^{18} e^-/cm^2 irradiated DND before (red) and after annealing (brown), both after boiling acid treatment, showing no significant difference in intensity.

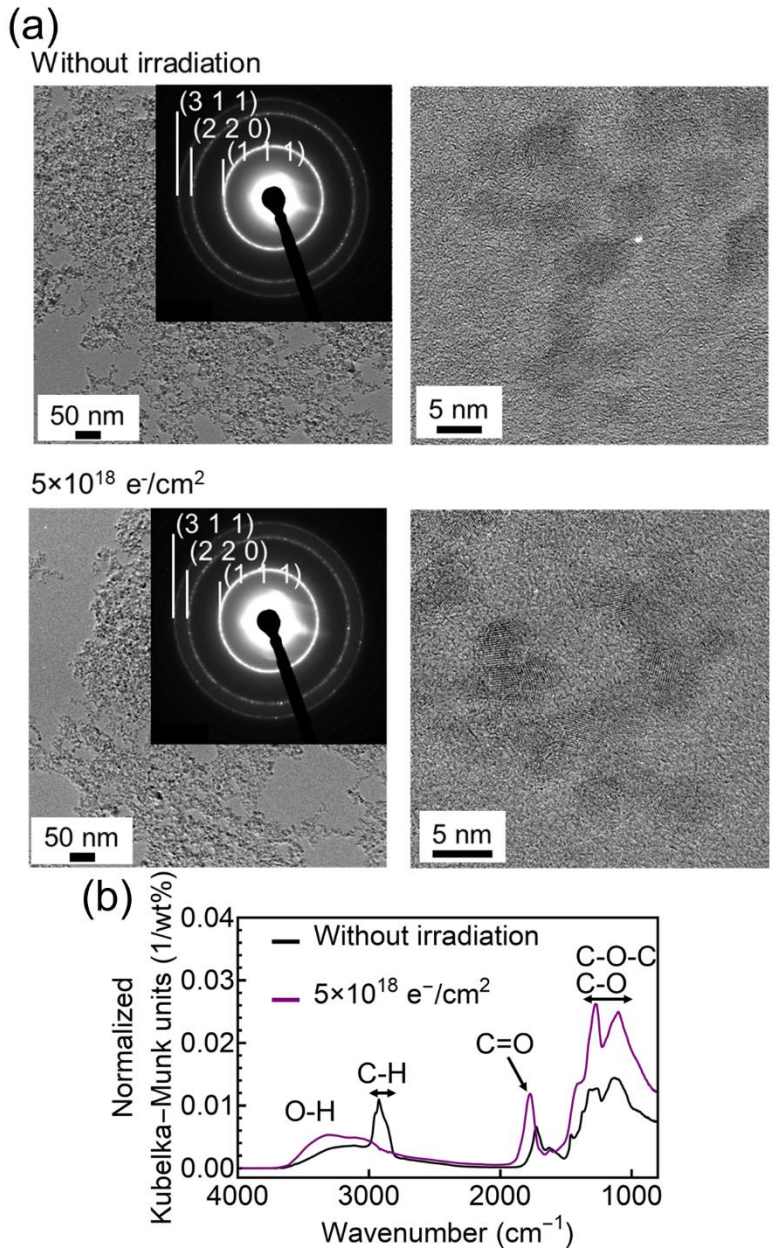

Figure 2. Effect of electron irradiation on the chemical structure of DND. (a) Transmission electron microscope (TEM) images with selected-area electron diffraction (SAED) for non-

irradiated DND (above) and 5×10^{18} e^-/cm^2 irradiated DND after the boiling acid treatment (below). (b) DRIFT spectra of non-irradiated DND (black) and 5×10^{18} e^-/cm^2 (purple) irradiated DND.

While the colloidal solution of DND (NanoCarbon Research Institute Co., Ltd., NanoAmando®) is mono-disperse with a hydrodynamic size of about 5 nm, the irradiated DND are strongly aggregated and cannot be dispersed in water by high-power sonication. Using dynamic light scattering (DLS), the irradiated DND show a broad peak stemming from aggregates (Fig. 3). To disperse the DND that aggregated during the electron irradiation, bead assisted sonic disintegration (BASD)[44,45] was first applied to the 1×10^{18} e^-/cm^2 irradiated DND. After a subsequent boiling acid treatment (H_2SO_4:HNO_3 = 3:1, 125 °C) a single peak centered at about 4-5 nm was regained (not shown). Since BASD was less effective for DND with higher fluences, we show that the electron irradiated DND can be fully disaggregated by the boiling acid treatment alone, without prior BASD (Fig. 3). This result confirms the successful production of dispersed single-digit electron irradiated DND. TEM images together with SAED showed that the size and structure of the nanodiamonds were retained after the boiling acid treatment (Fig. 2(a)). While BASD was not needed to disperse irradiated but not annealed DND, in contrast, annealed samples could only be disaggregated by applying the BASD process.

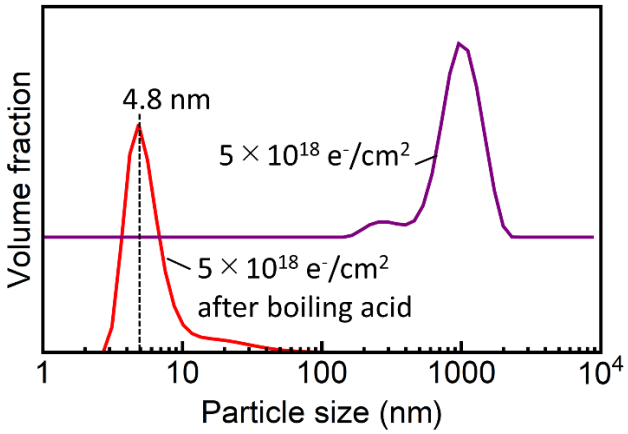

Figure 3. Characterization of the 5×10^{18} e^-/cm^2 irradiated DND before (purple) and after the boiling acid treatment (red). Hydrodynamic size distributions were measured by dynamic light scattering (DLS).

The oxidation treatment by the boiling acid method is not only important for the dispersion of the DND. Graphene or other sp^2 carbon units on the nanodiamond surface are known to have a significant influence on the optical properties of NV^- centers, namely the quenching of their fluorescence.[22] We have measured the fluorescence of the 1×10^{18} e^-/cm^2 irradiated DND with and without the boiling treatment using a homemade wide-field ODMR microscope[46]. We did not observe isolated DND but DND aggregates in these experiments. While the conventional fluorescence images showed a much larger intensity before the boiling acid treatment, "background-free NV^- center selective images"[46] showed bright spots only after the acid treatment (Fig. 4 (a)). Therefore, we can confirm the quenching of fluorescence from NV^- centers and its appearance after oxidation,[22] in our case by the boiling acid treatment. The observation of an NV^- signal is finally confirmed by recording an ODMR spectrum (Fig. 4 (b)).

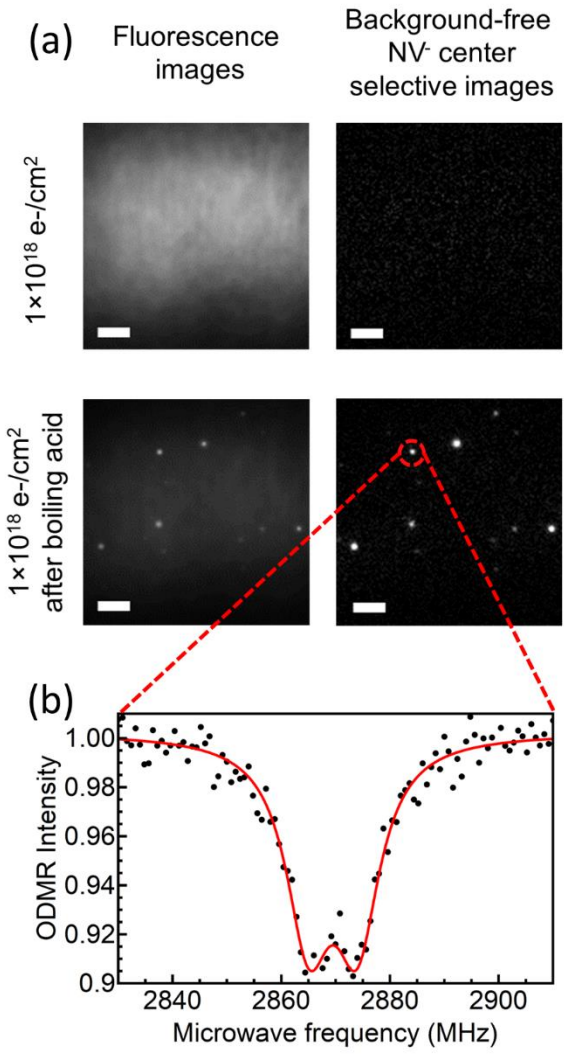

Figure 4. Effect on optical properties of irradiated DND before and after the boiling acid treatment. (a) Fluorescence images of dried DND aggregates on a glass cover slip, observed with a wide-field ODMR fluorescence microscope (532 nm laser irradiation); the left side shows conventional fluorescence images, the right side are background-free NV^- selective images.[46] While the unspecific fluorescence on the 1×10^{18} e^-/cm^2 irradiated DND before the boiling acid treatment is stronger (top row), spots with specific NV^- fluorescence do appear only after the boiling acid treatment (bottom row). The scale bar has a length of 5 μm. (b) ODMR spectrum from a bright

NV^- spot recorded by a microwave frequency sweep at zero magnetic field with a resonance frequency at about 2870 MHz.

CONCLUSIONS

Our results quantify for the first time the successful enrichment of NV^- centers in single-digit detonation nanodiamonds (DND), which can be maintained as a mono-disperse suspension in water. Hereby, we have addressed key challenges towards DND as single-digit "optical spin labels", which would enable magnetic resonance of a single biomolecule.

Using the EPR "half-field method", by observing the "forbidden" transition lines in the spectra of the negatively-charged NV^- defect ($S = 1$) in DND, we estimate a four-fold increase of the NV^--centers content in DND irradiated with an electron beam at a fluence of 5×10^{18} e^-/cm^2. This behavior is an experimental indication that there is a deficiency of vacancies with respect to nitrogen impurities in the diamond core of DND, which is in contrast to recent results obtained from electron energy-loss spectroscopy (EELS).[47] Electron irradiation with higher fluences are expected to further increase the concentration of NV^- centers in DND, since no saturation is yet seen in our series with three different fluences (Fig. 1 (a)). On the other hand, higher fluences may cause progressing radiation damage of the nanodiamond structure, a side effect that should be carefully analyzed. For the fluences applied in this work, the crystallinity of DND was not affected (Fig. 2(a)). Interestingly, we observe that the annealing process (800 °C for 2 h under vacuum) in the case of DND does not create any additional NV^- centers (Fig. 1 (a) and (c)). This concerns also the annealing of unprocessed DND without prior electron irradiation. Such an effect is unknown for bulk diamond or any other type of nanodiamonds and therefore a size-dependent origin seems

most reasonable. Further studies are required to elucidate the detailed mechanism. Independent of its theoretical understanding, this "negative result" leads to the practical advantage that the annealing step can be skipped for DND.

An absolute quantification of NV^- defects in DND is difficult. However, a careful estimation comparing with previously measured samples using the same half-field EPR method[31] suggests that the concentration of NV^- centers in initial (non-irradiated) DND under study is about 0.1 ppm (± 30%), which is equivalent in finding 1 per 1000 DND having an NV^- center. Consequently, DND irradiated with a fluence of 5×10^{18} e^-/cm^2 are expected to have an NV^- concentration of about 0.4 ppm (± 30%), where 1 in 250 DND should contain an NV^- center. This is 60 times higher than the yield of 1 per 15,000 DND particles determined by Plakhotnik and co-workers with optical methods.[22] Such a strong difference could stem from sample preparation (irradiation with 5×10^{15} protons/cm^2, 2.5 MeV in their work)[22], but more likely, it is originated from the different spectroscopic detection methods. In fact, while EPR measurements allow observation of all paramagnetic NV^- defects, fluorescence measurements of the same species may be subjected to laser-induced blinking or bleaching, which naturally limits its observation abilities.

The boiling acid treatment serves for three purposes in this work: (1) it disaggregates irradiated DND down to 4-5 nm, (2) it oxidizes surface groups to make the NV^- fluorescence and ODMR signal visible and (3) it removes contamination from Fe^{3+} enabling a nearly background-free half-field EPR spectrum[37] (see Fig. S2)). This confirms the importance of the surface oxidation step for the observation of NV^- fluorescence and ODMR reported previously[22] and shows that the boiling acid treatment is a reliable chemical tool for this purpose. We have observed strong NV^- fluorescence from dried DND aggregates after irradiation and the boiling acid treatment. As

proposed recently,[48] these could be used in their aggregated form as an alternative to HPHT nanodiamonds, now with a higher number of NV^- defects than in the unprocessed case.

As a final goal, we are aiming for isolated DND with a single NV^- center as an "optical spin label". Herein, we have presented two important steps towards this direction: our protocol can enrich detonation nanodiamonds in nitrogen-vacancy centers and re-disperse them to a size of 4-5 nm. We are convinced that the combination of both steps is pivotal for various future applications.

MATERIALS AND METHODS

Materials. A colloidal solution of DND (NanoCarbon Research Institute Co., Ltd., NanoAmando®) was kindly donated by Dr. Eiji Ōsawa. Zirconia beads (YTZ Grinding Media, 0.05 mm) were obtained from Tosoh Co.

Characterization. DRIFT spectra were obtained on a FT/IR-6600 (JASCO) equipped with diffuse reflectance accessory (DR PRO410-M) with a resolution of 4 cm^{-1}. The DND samples and KBr (1:1, w/w) were grinded using mortar and pestle. Adsorbed water in the powder was removed by heating at 120 ºC under vacuum for 1h. The dried powder was subsequently filled into the reflectance cup and flattened with the spatula. The reflectance cup was placed into the chamber and the air was replaced with nitrogen gas. Measurements were performed with 64 scans at a resolution of 4 cm^{-1}. A linear background correction, based on the maximum value of the diffuse reflectance R (raw data) in the region of 3800 - 4000 cm^{-1} was applied to the spectra. After the background correction, the Kubelka-Munk equation (Kubelka-Munk units = $(1-R)^2/2R$) was applied to the spectra. To correct the data for the slightly different concentration in DND, the horizontal axis was normalized by the concentration of the DND samples. Zeta potentials and the

hydrodynamic size distributions of the samples were measured using a Malvern Zeta sizer Nano instrument (Malvern Panalytical Ltd). Transmission electron microscopy (TEM) images were obtained by a FEM-2200FS+CEOS CETCOR (JEOL). The acceleration voltage and the spatial resolution was 200 kV and 0.1 nm, respectively.

Irradiation and annealing process. A freeze-dried detonation nanodiamond powder was irradiated with a 2-MeV electron beam at a fluence of 1×10^{18} e^-/cm^{-2} (50 h), 3×10^{18} e^-/cm^2 (150 h) and 5×10^{18} e^-/cm^2 (250 h). The thermal annealing was carried out under vacuum at 800 °C for 2 h.

Bead assisted sonic disintegration (BASD) process. The reactor was charged with DND powder (150 mg), zirconia beads (10 g), a stirring bar and milli-Q water (10 ml) before the homogenizer tip were immersed. The prepared sample was sonicated using an ultrasonic processor (Branson, Ultrasonic-Homogenizer Sonifier 450A with a 5 mm microtip EDP No. 101-148-069) for 2 h at the output control 6 and a duty cycle of 10 % or 30 % while stirring and cooling the reactor. After sonication, the mixture was centrifuged (TOMY, MX-300) at 5 krpm for 10 min at room temperature and the supernatant was discarded. This was repeated three times to completely remove the remaining zirconia beads.

Boiling acid treatment. 100 mg of aqueous colloidal solution of DND were centrifuged (Beckman, Optima™ TLX ultracentrifuge) at 50 krpm for 30 min at 25 °C, the supernatant was discarded and 20 ml mixture of sulfuric acid and nitric acid (3:1) were added (for irradiated DND powders, the centrifugation step was skipped). The suspension was transferred to a flask and sonicated in an ice bath sonication (Cosmo Bio, Bioruptor UCS-200TM) (on/off=10 s/5 s) for 30 min. The mixture was heated under reflux at 125 °C and stirred for 3 or 5 days. After the reaction,

the mixture was washed three times with milli-Q water. Next, the sample was treated with a 0.1 M NaOH solution (20 ml) at 90 ºC for 2 h. Only for the annealed samples, this step was followed by washing with a 0.1 M HCl solution (20 ml) at 90 ºC for 2 h. The sample was dispersed again in milli-Q water (20 ml) by using an ultrasonic processor for 30 min at the output control 5 with a duty cycle of 30 % while stirring and cooling the reactor.

Electron paramagnetic resonance (EPR). Continuous-wave X-band EPR spectra were recorded on a Bruker ELEXSYS E500 spectrometer at room temperature and are plotted as derivative spectra. A tube was filled with 20 mg of DND powder and spectra were acquired for about 3 h. A microwave frequency of 9.87 GHz at a power level of 0.2 mW was applied and 1024 points around a magnetic field of 165 mT with a sweep width of 50mT were acquired. The modulation amplitude was 0.3 mT and the modulation frequency 100 kHz. All samples were previously treated by "boiling acid" to remove Fe^{3+} contaminations on the DND usually causing appearance of strong broad background EPR lines within the same field range.[37] The residual background Fe^{3+} line was removed by post-processing. The relative amount of NV^- defects was determined by the double integration of the signal with a resulting value normalized per unit mass. The error of ± 15% stems from the spectral noise and the background correction. EPR data processing was carried out using Bruker WIN-EPR and OriginLab software packages and is illustrated in Fig. S3. The frequency-dependent *g*-value of the $\Delta M_S = 2$ transition in the NV^- center was calculated using the function "pepper" in EasySpin running on MATLAB.[49] The quantification of the NV^- centers content was done by comparison of the double-integrated intensities of the $g = 4.24(1)$ EPR lines in all the samples studied with that of a fluorescent microdiamond sample having an NV^- content of 10.8 ppm. The latter value was reported in Ref. [31] for this sample, which we used as a reference. All NV^- densities there[31] were obtained by an "EPR-only" technique based on the direct double

integration of the entire polycrystalline NV^- related pattern (including signals of both "allowed" and "forbidden" transitions) and its quantification using external polycrystalline EPR reference sample with a known spin density.[37] Integral intensities of the "forbidden" $g = 4.24(1)$ signal are proportional to the NV^- contents determined by the double integration of the entire triplet signals, which allows estimating of the NV^- content even in cases where the "allowed" transitions' signals are obscured or not observable.[31]

Fluorescence and ODMR measurements. Fluorescence and NV^- selective images were recorded using a homemade ODMR microscope reported previously.[46] The samples were excited with an Nd:YAG laser (532 nm, Coherent, Sapphire 532 LP), and the fluorescence was collected by an oil immersion 60× objective (ApoTIRF, NA = 1.49, Nikon), passed through a dichroic mirror centered at 575 nm and a long-wave (short-wave) pass filter between 590 nm and 845 nm to detect the fluorescence of NV^- before imaged at an EMCCD camera (Andor Technology, Andor iXon Ultra 897). Fluorescence spectra were recorded by placing an imaging spectrograph (Bunkou Keiki CLP-50, 0.5 nm resolution) between the microscope and the camera. The microscope was equipped with a microwave coil for irradiating the resonant frequency and the ODMR spectrum was recorded with a microwave frequency sweep from 2830 to 2910 MHz. Two Cauchy distribution functions were applied to fit the data. To plot the background-free NV^- selective images, fluorescence images with and without a resonant microwave frequency at 2870 MHz were alternated and subtracted from each other.[46]

Supporting Information Available: All EPR spectra (Fig. S1), unprocessed EPR spectra for different duration of boiling acid treatment (Fig. S2), illustration of the background correction and integration procedure of the EPR spectra (Fig. S3) and further DRIFT spectra (Fig. S4).

This material is available free of charge via the Internet at http://pubs.acs.org.

Supporting Information (PDF)

AUTHOR INFORMATION

Corresponding Author

* E-mail: segawat@ethz.ch

Author Contributions

The manuscript was written through contributions of all authors. All authors have given approval to the final version of the manuscript.

Funding Sources

- The Branco Weiss Fellowship - Society in Science
- Japan Agency for Medical Research and Development (AMED), Grant No. JP16gm0510004
- JSPS KAKENHI, Grant Numbers JP26119004 and JP15K21711

ACKNOWLEDGMENT

T.F.S. acknowledges The Branco Weiss Fellowship - Society in Science, administered by the ETH Zurich and Prof. Shirakawa for hosting him as a Guest Research Associate at Kyoto University. TEM images were acquired at the Kyoto University Nanotechnology Platform by the expertise of Prof. Kurota and Dr. Kiyomura. Profs. Akiyoshi/Mukai and Prof. Mizuochi are all kindly

acknowledged for their access to the DLS setup and EPR spectrometer, respectively. Mr. Takami and Mr. Watanabe, JASCO Co., are kindly acknowledged for their help in recording the DRIFT spectra and Dr. Hara, Bruker Japan, is kindly acknowledged for help with preliminary EPR measurements. This research was supported by the Japan Agency for Medical Research and Development (AMED), Grant No. JP16gm0510004 and JSPS KAKENHI, Grant Numbers JP26119004 and JP15K21711, including a Fund for International Collaboration on a Grant-in-Aid for Scientific Research on Innovative Areas for T.F.S. We thank Prof. Mizuochi and Dr. Sotoma for stimulating discussions, Dr. Morishita for help with the EPR spectrometer and Mr. Frederick So for the careful reading of the manuscript.

ABBREVIATIONS

DLS, dynamic light scattering; DND, detonation nanodiamond; DRIFTS, diffuse reflectance infrared Fourier transform spectroscopy; EPR, electron paramagnetic resonance; NV^- center, negatively-charged nitrogen-vacancy center; NV^0 center, neutral nitrogen-vacancy center; ODMR, optically-detected magnetic resonance; SAED, selected-area electron diffraction; TEM, transmission electron microscopy.

REFERENCES

(1) Gruber, A.; Dräbenstedt, A.; Tietz, C.; Fleury, L.; Wrachtrup, J.; Borczyskowski, C. Scanning Confocal Optical Microscopy and Magnetic Resonance on Single Defect Centers. *Science* **1997**, *276*, 2012–2014.

(2) Jelezko, F.; Gaebel, T.; Popa, I.; Gruber, A.; Wrachtrup, J. Observation of Coherent Oscillations in a Single Electron Spin. *Phys. Rev. Lett.* **2004**, *92*, 076401.

(3) Balasubramanian, G.; Neumann, P.; Twitchen, D.; Markham, M.; Kolesov, R.; Mizuochi, N.; Isoya, J.; Achard, J.; Beck, J.; Tissler, J.; et al. Ultralong Spin Coherence Time in Isotopically Engineered Diamond. *Nat. Mater.* **2009**, *8*, 383–387.

(4) Wrachtrup, J.; Finkler, A. Single Spin Magnetic Resonance. *J. Magn. Reson.* **2016**, *269*, 225–236.

(5) Acosta, V. M.; Bauch, E.; Ledbetter, M. P.; Waxman, A.; Bouchard, L.; Budker, D. Temperature Dependence of the Nitrogen-Vacancy Magnetic Resonance in Diamond. *Phys. Rev. Lett.* **2010**, *104*, 070801.

(6) Plakhotnik, T.; Doherty, M. W.; Cole, J. H.; Chapman, R.; Manson, N. B. All-Optical Thermometry and Thermal Properties of the Optically Detected Spin Resonances of the NV-Center in Nanodiamond. *Nano Lett.* **2014**, *14*, 4989–4996.

(7) Maze, J. R.; Stanwix, P. L.; Hodges, J. S.; Hong, S.; Taylor, J. M.; Cappellaro, P.; Jiang, L.; Dutt, M. V. G.; Togan, E.; Zibrov, A. S.; et al. Nanoscale Magnetic Sensing with an

Individual Electronic Spin in Diamond. *Nature* **2008**, *455*, 644–647.

(8) Balasubramanian, G.; Chan, I. Y.; Kolesov, R.; Al-Hmoud, M.; Tisler, J.; Shin, C.; Kim, C.; Wojcik, A.; Hemmer, P. R.; Krueger, A.; et al. Nanoscale Imaging Magnetometry with Diamond Spins under Ambient Conditions. *Nature* **2008**, *455*, 648–651.

(9) Dolde, F.; Fedder, H.; Doherty, M. W.; Nöbauer, T.; Rempp, F.; Balasubramanian, G.; Wolf, T.; Reinhard, F.; Hollenberg, L. C. L.; Jelezko, F.; et al. Electric-Field Sensing Using Single Diamond Spins. *Nat. Phys.* **2011**, *7*, 459–463.

(10) Schirhagl, R.; Chang, K.; Loretz, M.; Degen, C. L. Nitrogen-Vacancy Centers in Diamond: Nanoscale Sensors for Physics and Biology. *Annu. Rev. Phys. Chem.* **2014**, *65*, 83–105.

(11) Yu, S.-J.; Kang, M.-W.; Chang, H.-C.; Chen, K.-M.; Yu, Y.-C. Bright Fluorescent Nanodiamonds: No Photobleaching and Low Cytotoxicity. *J. Am. Chem. Soc.* **2005**, *127*, 17604–17605.

(12) McGuinness, L. P.; Yan, Y.; Stacey, A.; Simpson, D.; Hall, L. T.; Maclaurin, D.; Prawer, S.; Mulvaney, P.; Wrachtrup, J.; Caruso, F.; et al. Quantum Measurement and Orientation Tracking of Fluorescent Nanodiamonds inside Living Cells. *Nat. Nanotechnol.* **2011**, *6*, 358–363.

(13) Kucsko, G.; Maurer, P. C.; Yao, N. Y.; Kubo, M.; Noh, H. J.; Lo, P. K.; Park, H.; Lukin, M. D. Nanometre-Scale Thermometry in a Living Cell. *Nature* **2013**, *500*, 54–58.

(14) Terada, D.; Sotoma, S.; Harada, Y.; Igarashi, R.; Shirakawa, M. One-Pot Synthesis of Highly Dispersible Fluorescent Nanodiamonds for Bioconjugation. *Bioconjug. Chem.* **2018**,

29, 2786–2792.

(15) Ormö, M.; Cubitt, A. B.; Kallio, K.; Gross, L. A.; Tsien, R. Y.; Remington, S. J. Crystal Structure of the Aequorea Victoria Green Fluorescent Protein. *Science* **1996**, *273*, 1392–1395.

(16) Hubbell, W. L.; Cafiso, D. S.; Altenbach, C. Identifying Conformational Changes with Site-Directed Spin Labeling. *Nat. Struct. Biol.* **2000**, *7*, 735–739.

(17) Hsiao, W. W. W.; Hui, Y. Y.; Tsai, P. C.; Chang, H. C. Fluorescent Nanodiamond: A Versatile Tool for Long-Term Cell Tracking, Super-Resolution Imaging, and Nanoscale Temperature Sensing. *Acc. Chem. Res.* **2016**, *49*, 400–407.

(18) Sotoma, S.; Terada, D.; Segawa, T. F.; Igarashi, R.; Harada, Y.; Shirakawa, M. Enrichment of ODMR-Active Nitrogen-Vacancy Centres in Five-Nanometre-Sized Detonation-Synthesized Nanodiamonds: Nanoprobes for Temperature, Angle and Position. *Sci. Rep.* **2018**, *8*, 1–8.

(19) Krüger, A.; Kataoka, F.; Ozawa, M.; Fujino, T.; Suzuki, Y.; Aleksenskii, A. E.; Vul', A. Y.; Ōsawa, E. Unusually Tight Aggregation in Detonation Nanodiamond : Identification and Disintegration. *Carbon* **2005**, *43*, 1722–1730.

(20) Pauzauskie, P. J.; Crowhurst, J. C.; Worsley, M. A.; Laurence, T. A.; Kilcoyne, A. L. D.; Wang, Y.; Willey, T. M.; Visbeck, K. S.; Fakra, S. C.; Evans, W. J.; et al. Synthesis and Characterization of a Nanocrystalline Diamond Aerogel. *Proc. Natl. Acad. Sci. U. S. A.* **2011**, *108*, 8550–8553.

(21) Smith, B. R.; Inglis, D. W.; Sandnes, B.; Rabeau, J. R.; Zvyagin, A. V.; Gruber, D.; Noble, C. J.; Vogel, R.; Ōsawa, E.; Plakhotnik, T. Five-Nanometer Diamond with Luminescent Nitrogen-Vacancy Defect Centers. *Small* **2009**, *5*, 1649–1653.

(22) Smith, B. R.; Gruber, D.; Plakhotnik, T. The Effects of Surface Oxidation on Luminescence of Nano Diamonds. *Diam. Relat. Mater.* **2010**, *19*, 314–318.

(23) Dolmatov, V. Y. Detonation Synthesis Ultradispersed Diamonds: Properties and Applications. *Russ. Chem. Rev.* **2001**, *70*, 607–626.

(24) Fang, X.; Mao, J.; Levin, E. M.; Schmidt-Rohr, K. Nonaromatic Core-Shell Structure of Nanodiamond from Solid-State NMR Spectroscopy. *J. Am. Chem. Soc.* **2009**, *131*, 1426–1435.

(25) Turner, S.; Lebedev, O. I.; Shenderova, O.; Vlasov, I. I.; Verbeeck, J.; Van Tendeloo, G. Determination of Size, Morphology, and Nitrogen Impurity Location in Treated Detonation Nanodiamond by Transmission Electron Microscopy. *Adv. Funct. Mater.* **2009**, *19*, 2116–2124.

(26) Turner, S.; Shenderova, O.; Da Pieve, F.; Lu, Y. G.; Yücelen, E.; Verbeeck, J.; Lamoen, D.; Van Tendeloo, G. Aberration-Corrected Microscopy and Spectroscopy Analysis of Pristine, Nitrogen Containing Detonation Nanodiamond. *Phys. Status Solidi Appl. Mater. Sci.* **2013**, *210*, 1976–1984.

(27) Tisler, J.; Balasubramanian, G.; Naydenov, B.; Kolesov, R.; Grotz, B.; Reuter, R.; Boudou, J. P.; Curmi, P. A.; Sennour, M.; Thorel, A.; et al. Fluorescence and Spin Properties of Defects in Single Digit Nanodiamonds. *ACS Nano* **2009**, *3*, 1959–1965.

(28) Bradac, C.; Gaebel, T.; Naidoo, N.; Sellars, M. J.; Twamley, J.; Brown, L. J.; Barnard, A. S.; Plakhotnik, T.; Zvyagin, A. V; Rabeau, J. R. Observation and Control of Blinking Nitrogen-Vacancy Centres in Discrete Nanodiamonds. *Nat. Nanotechnol.* **2010**, *5*, 345–349.

(29) Rondin, L.; Dantelle, G.; Slablab, A.; Grosshans, F.; Treussart, F.; Bergonzo, P.; Perruchas, S.; Gacoin, T.; Chaigneau, M.; Chang, H. C.; et al. Surface-Induced Charge State Conversion of Nitrogen-Vacancy Defects in Nanodiamonds. *Phys. Rev. B - Condens. Matter Mater. Phys.* **2010**, *82*, 115449.

(30) Vlasov, I. I.; Shenderova, O.; Turner, S.; Lebedev, O. I.; Basov, A. A.; Shiryaev, A. A.; Tendeloo, G. Van; Sildos, I.; Rähm, M.; Shiryaev, A. A.; et al. Nitrogen and Luminescent Nitrogen-Vacancy Defects in Detonation Nanodiamond. *Small* **2010**, *6*, 687–694.

(31) Shames, A. I.; Osipov, V. Y.; Boudou, J. P.; Panich, A. M.; von Bardeleben, H. J.; Treussart, F.; Vul', A. Y. Magnetic Resonance Tracking of Fluorescent Nanodiamond Fabrication. *J. Phys. D. Appl. Phys.* **2015**, *48*, 155302.

(32) Qin, L.; Iijima, S. Onion-like Graphitic Particles Produced from Diamond. *Chem. Phys. Lett.* **1996**, *262*, 252–258.

(33) Kis, A.; Csányi, G.; Salvetat, J. P.; Lee, T. N.; Couteau, E.; Kulik, A. J.; Benoit, W.; Brugger, J.; Forró, L. Reinforcement of Single-Walled Carbon Nanotube Bundles by Intertube Bridging. *Nat. Mater.* **2004**, *3*, 153–157.

(34) Krasheninnikov, A. V.; Nordlund, K. Ion and Electron Irradiation-Induced Effects in Nanostructured Materials. *J. Appl. Phys.* **2010**, *107*, 071301.

(35) Havlik, J.; Petrakova, V.; Rehor, I.; Petrak, V.; Gulka, M.; Stursa, J.; Kucka, J.; Ralis, J.; Rendler, T.; Lee, S. Y.; et al. Boosting Nanodiamond Fluorescence: Towards Development of Brighter Probes. *Nanoscale* **2013**, *5*, 3208–3211.

(36) Osswald, S.; Yushin, G.; Mochalin, V.; Kucheyev, S. O.; Gogotsi, Y. Control of sp^2/sp^3 Carbon Ratio and Surface Chemistry of Nanodiamond Powders by Selective Oxidation in Air. *J. Am. Chem. Soc.* **2006**, *128*, 11635–11642.

(37) Osipov, V. Y.; Shames, A. I.; Enoki, T.; Takai, K.; Baidakova, M. V.; Vul', A. Y. Paramagnetic Defects and Exchange Coupled Spins in Pristine Ultrananocrystalline Diamonds. *Diam. Relat. Mater.* **2007**, *16*, 2035–2038.

(38) Shames, A. I.; Osipov, V. Y.; von Bardeleben, H. J.; Boudou, J. P.; Treussart, F.; Vul', A. Y. Native and Induced Triplet Nitrogen-Vacancy Centers in Nano- and Micro-Diamonds: Half-Field Electron Paramagnetic Resonance Fingerprint. *Appl. Phys. Lett.* **2014**, *104*, 063107.

(39) van der Waals, J. H.; de Groot, M. S. Paramagnetic Resonance in Phosphorescent Aromatic Hydrocarbons. I: Naphthalene. *Mol. Phys.* **1959**, *2*, 333–340.

(40) Felton, S.; Edmonds, A. M.; Newton, M. E.; Martineau, P. M.; Fisher, D.; Twitchen, D. J. Electron Paramagnetic Resonance Studies of the Neutral Nitrogen Vacancy in Diamond. *Phys. Rev. B* **2008**, *77*, 081201.

(41) Boudou, J. P.; Curmi, P. A.; Jelezko, F.; Wrachtrup, J.; Aubert, P.; Sennour, M.; Balasubramanian, G.; Reuter, R.; Thorel, A.; Gaffet, E. High Yield Fabrication of Fluorescent Nanodiamonds. *Nanotechnology* **2009**, *20*, 235602.

(42) Chen, G. Nonlocal and Nonequilibrium Heat Conduction in the Vicinity of Nanoparticles. *J. Heat Transfer* **1996**, *118*, 539–545.

(43) Osipov, V. Y.; Aleksenskiy, A. E.; Shames, A. I.; Panich, A. M.; Shestakov, M. S.; Vul, A. Y. Infrared Absorption Study of Surface Functional Groups Providing Chemical Modification of Nanodiamonds by Divalent Copper Ion Complexes. *Diam. Relat. Mater.* **2011**, *20*, 1234–1238.

(44) Ozawa, M.; Inaguma, M.; Takahashi, M.; Kataoka, F.; Krüger, A.; Ōsawa, E. Preparation and Behavior of Brownish, Clear Nanodiamond Colloids. *Adv. Mater.* **2007**, *19*, 1201–1206.

(45) Liang, Y.; Ozawa, M.; Krueger, A. A General Procedure to Functionalize Agglomerating Nanoparticles Demonstrated on Nanodiamond. *ACS Nano* **2009**, *3*, 2288–2296.

(46) Igarashi, R.; Yoshinari, Y.; Yokota, H.; Sugi, T.; Sugihara, F.; Ikeda, K.; Sumiya, H.; Tsuji, S.; Mori, I.; Tochio, H.; et al. Real-Time Background-Free Selective Imaging of Fluorescent Nanodiamonds in Vivo. *Nano Lett.* **2012**, *12*, 5726–5732.

(47) Chang, S. L. Y.; Barnard, A. S.; Dwyer, C.; Boothroyd, C. B.; Hocking, R. K.; Osawa, E.; Nicholls, R. J. Counting Vacancies and Nitrogen-Vacancy Centers in Detonation Nanodiamond. **2016**, *8*, 10548–10552.

(48) Reineck, P.; Capelli, M.; Lau, D. W. M.; Jeske, J.; Field, M. R.; Ohshima, T.; Greentree, A. D.; Gibson, B. C. Bright and Photostable Nitrogen-Vacancy Fluorescence from Unprocessed Detonation Nanodiamond. *Nanoscale* **2017**, *9*, 497–502.

(49) Stoll, S.; Schweiger, A. EasySpin, a Comprehensive Software Package for Spectral Simulation and Analysis in EPR. *J. Magn. Reson.* **2006**, *178*, 42–55.